A Functional Description of the Buffered Telemetry Demodulator (BTD)

H. Tsou, B. Shah, R. Lee, and S. Hinedi
Communications Systems Research Section

This article gives a functional description of the buffered telemetry demodulator (BTD), which operates on recorded digital samples to extract the symbols from the received signal. The key advantages of the BTD are (1) its ability to reprocess the signal to reduce acquisition time, (2) its ability to use future information about the signal and to perform smoothing on past samples, and (3) its minimum transmission bandwidth requirement as each subcarrier harmonic is processed individually. The first application of the BTD would be the Galileo S-band contingency mission, where the signal is so weak that reprocessing to reduce the acquisition time is crucial. Moreover, in the event of employing antenna arraying with full spectrum combining, only the subcarrier harmonics need to be transmitted between sites, resulting in significant reduction in data rate transmission requirements. Software implementation of the BTD is described for various general-purpose computers.

I. Introduction

Current DSN receivers operate on the received signal in real time and do not buffer or store the received signal for reprocessing. As a result, data lost during acquisition or cycle slips is not recoverable. In some DSN missions, the link margin is so low that signal acquisition (carrier, subcarrier, and symbol) takes too long, resulting in significant data loss. Such a scenario occurs during operation at low data rates (on the order of a few hundred symbols per second) with rate 1/4, 1/5, and 1/6 convolutional codes, resulting in symbol signal-to-noise ratios (SNR's) between −4 dB and −6 dB. This combination of low symbol SNR and low data rate produces unusually long acquisition times dominated by the behavior of the subcarrier- and symbol-synchronization loops. The acquisition time can, in some instances, be as long as 20 minutes and depends on the scenario of interest. The problem is augmented when suppressed carriers are employed, since the Costas loop SNR is a nonlinear function of the symbol SNR; significant squaring loss results. When the data rate on the spacecraft is programmed to take advantage of the antenna aperture on the ground, several data rate changes can occur in a pass or a single day, each resulting in data loss due to resynchronization in the ground receiver.

The buffered telemetry demodulator (BTD) overcomes these problems by recording the signal and then processing and reprocessing the samples. Once acquisition occurs, the BTD can operate on the past data, using estimates of the signal state (such as phase, frequency, and Doppler rate) to basically go back in time and recover those symbols lost during acquisition. This is referred to as smoothing,

where "future" data are used to provide an estimate in the "past." The optimum strategy on the data playback is still under investigation and will be the topic of a future report. The BTD is designed mainly for low-data-rate applications and can be implemented on a general-purpose workstation. In order to reduce the computational requirement, the signal is recorded on a subcarrier harmonic basis, thus rendering the BTD independent of the subcarrier frequency. This results in a computational throughput requirement based on the data rate rather than on the bandwidth of the transmitted signal. In addition, when antenna arraying is employed and full spectrum combining is utilized, only a fraction of the total signal bandwidth needs to be transmitted between sites, resulting in significant reduction in transmission requirements. In this article, the BTD is functionally described and its implementation on various workstations is evaluated. First, the carrier and subcarrier synchronization loops are reviewed. Then, the recording of the signal is described; each subcarrier harmonic is individually demodulated to baseband and recorded. Finally, the coherent baseband demodulation is discussed along with requirements for software implementation of the BTD. Also, a glossary is included.

II. A Review of the Advanced Receiver Carrier and Subcarrier Loops

The advanced receiver II (ARX II) [1] is a receiving system that has been developed to digitally demodulate and process signals from deep-space spacecraft. It is a breadboard system for the Block V receiver, which will eventually replace various receivers currently used in the DSN [2]. This section briefly reviews the ARX II carrier and subcarrier loops so that they can be compared to the carrier and subcarrier loops of the BTD. The main difference between the ARX II and BTD is that the ARX II carrier and subcarrier loops process the received signal after it has been open-loop downconverted to an intermediate frequency (IF), whereas the BTD loops process the received signal after it has been open-loop downconverted to baseband on a subcarrier harmonic basis. All the other receiving functions, e.g., symbol synchronization, symbol detection, lock detection, etc., are implemented the same way in both the ARX II and BTD. Consequently, they are not discussed in this article. Instead, the interested reader is referred to [1] for a complete review of these functions.

A block diagram of the ARX II carrier and subcarrier loops is shown in Fig. 1. The received signal, which is assumed to be a typical deep space signal, consists of a residual sinusoidal carrier and a square-wave subcarrier. After downconversion to an appropriate IF, it can be represented as

$$r(t) = \sqrt{2P}\cos(\Delta)\sin[\Psi_c(t)] + \sqrt{2P}\sin(\Delta)d(t)\ \mathrm{sgn}\{\sin[\Psi_{su}(t)]\} \times \cos[\Psi_c(t)] + n(t) \quad (1)$$

where $P_c = P\cos^2(\Delta)$ and $P_d = P\sin^2(\Delta)$ in watts are the received carrier power and data power, respectively; $\Psi_c(t)$ is the total carrier phase; and $\Psi_{su}(t)$ is the total subcarrier phase, both in radians. The data, $d(t)$, are given by

$$d(t) = \sum_{l=-\infty}^{\infty} a_l p(t - lT) \quad (2)$$

where $p(t)$ is the unit-power square pulse limited to T seconds and $\{a_l\}$ represents the independent and equally likely binary (± 1) symbols. The noise process, $n(t)$, is modeled as bandpass with a flat, one-sided power spectral density (PSD) level equal to N_0 W/Hz. By expressing the square-wave subcarrier as an infinite sum, i.e.,

$$\mathrm{sgn}\{\sin[\Psi_{su}(t)]\} = \frac{4}{\pi}\sum_{\substack{j=1 \\ j:odd}}^{\infty}\frac{1}{j}\sin[j\Psi_{su}(t)] \quad (3)$$

the digitized signal, which is sampled at rate $R_s = 1/T_s$, can be written as

$$r(kT_s) = \sqrt{2P_c}\sin[\Psi_c(kT_s)] + \sqrt{2P_d}d(kT_s)\left(\frac{4}{\pi}\sum_{\substack{j=1 \\ j:odd}}^{L}\frac{\sin[j\Psi_{su}(kT_s)]}{j}\right) \times \cos[\Psi_c(kT_s)] + n(kT_s) \quad (4)$$

where only up to the Lth subcarrier harmonics (L is an odd integer) are assumed to be present at the analog-to-digital (A/D) converter output in Fig. 1. Samples of the bandpass noise can be expressed as

$$n(kT_s) = \sqrt{2}n_1(kT_s)\cos[\Psi_c(kT_s)] - \sqrt{2}n_2(kT_s)\sin[\Psi_c(kT_s)] \quad (5)$$

where the random variables $n_1(kT_s)$ and $n_2(kT_s)$ are samples of the baseband noise processes $n_1(t)$ and $n_2(t)$, which are assumed to be statistically independent, white Gaussian noise processes with a flat, one-sided PSD level equal to N_0 W/Hz within a one-sided bandwidth equal to $1/(2T_s)$ Hz. As a result, $n_1(kT_s)$ and $n_2(kT_s)$ are zero-mean with variance $\sigma_{n_1}^2 = \sigma_{n_2}^2 = N_0/(2T_s)$. The time index kT_s will now be omitted to allow a simpler notation.

The residual carrier tracking loop control signal, U_q in Fig. 1, is derived by mixing the digitized IF signal with its carrier quadrature component, lowpass filtering the mixer output, and then accumulating the filtered samples over the loop update interval. Mathematically,

$$U_q = \sqrt{P_c}\sin(\phi_c) + n_{U_q} \tag{6}$$

where ϕ_c is the carrier phase error, n_{U_q} is a zero-mean Gaussian random variable with variance $N_0/(2T_u)$, and $T_u = M_1T_s$ is the loop update interval in seconds. Note that the data have been neglected in writing Eq. (6), since it is assumed that the accumulator in the carrier quadrature arm averages over several subcarrier cycles (i.e., $f_{su}T_u \gg 1$) and that the data sum is thus approximately zero. It will be shown in Section IV that the BTD carrier loop control signal has the same signal power and noise statistics as Eq. (6) and, therefore, both loops will have the same tracking performance.

Next, consider the subcarrier tracking loop. As shown in Fig. 1, the input to the subcarrier loop is the quadrature component of the residual carrier. The subcarrier control signal is obtained by forming the product $Z_iZ_{q,su}$, where Z_i is the output of the subcarrier inphase arm and $Z_{q,su}$ is the output of the subcarrier quadrature arm. Note that the subscript "*su*" in $Z_{q,su}$ is used to distinguish it from $Z_{q,sca}$, the quadrature arm of the suppressed carrier loop. The signals Z_i and $Z_{q,su}$ are obtained after mixing the residual carrier quadrature component with, respectively, the subcarrier inphase and quadrature references and then accumulating these samples over a symbol duration (perfect symbol synchronization assumed). These signals are given as [1]

$$Z_i = \sqrt{P_d}a_lF_I(\phi_{su})\cos(\phi_c) + n_{Z_i} \tag{7}$$

and

$$Z_{q,su} = \sqrt{P_d}a_lF_Q(\phi_{su})\cos(\phi_c) + n_{Z_{q,su}} \tag{8}$$

where ϕ_{su} is the subcarrier phase error and the functions $F_I(\phi_{su})$ and $F_Q(\phi_{su})$ are periodic functions of ϕ_{su} (period 2π) given in the principal phase interval $[-\pi, \pi]$ as follows [1]:

$$F_I(\phi_{su}) = 1 - \frac{2}{\pi}|\phi_{su}|, \quad |\phi_{su}| \le \pi \tag{9}$$

and

$$F_Q(\phi_{su}) = \begin{cases} (2/\pi)\phi_{su} & |\phi_{su}| \le (\pi/2)W_{su} \\ \mathrm{sgn}(\phi_{su})W_{su} & (\pi/2)W_{su} \le |\phi_{su}| < \pi(1 - W_{su}/2) \\ 2\mathrm{sgn}(\phi_{su}) - (2/\pi)\phi_{su} & \pi(1 - W_{su}/2) \le |\phi_{su}| \le \pi \end{cases} \tag{10}$$

The parameter W_{su}, in fractions of cycles, is the width of the subcarrier window ($W_{su} \le 1$, and $W_{su} = 1$ corresponds to the "no window" case). It is used in the quadrature arm to improve the square-wave tracking performance [3]. The noises n_{Z_i} and $n_{Z_{q,su}}$ in Eqs. (7) and (8) are independent with respective variances $N_0/(2T)$ and $N_0W_{su}/(2T)$, where T denotes symbol duration. It will be shown in Section IV that the BTD inphase and quadrature accumulator outputs have the same signal and noise statistics as Eqs. (7) and (8). Consequently, both subcarrier loops will have the same control signal and, therefore, the same tracking performance.

Finally, consider the case of the suppressed carrier with subcarrier ($\Delta = 90$ deg in Eq. [1]). In this scenario, the suppressed carrier loop control signal is obtained by form-

ing the product $Z_i Z_{q,sca}$, as shown in Fig. 1. The signal Z_i, which was shown to be the subcarrier inphase component, now becomes the suppressed carrier inphase component because it is already proportional to $\cos(\phi_c)$ and $F_I(\phi_{su})$, as indicated by Eq. (7). The suppressed carrier quadrature component $Z_{q,sca}$ is generated by mixing the digitized IF signal with the quadrature carrier reference and the inphase subcarrier reference, and then accumulating the resulting samples over a symbol duration. Hence, the suppressed carrier inphase and quadrature signals are given as [1]

$$Z_i = \sqrt{P_d} a_l F_I(\phi_{su}) \cos(\phi_c) + n_{Z_i} \tag{11}$$

and

$$Z_{q,sca} = \sqrt{P_d} a_l F_I(\phi_{su}) \sin(\phi_c) + n_{Z_{q,sca}} \tag{12}$$

where n_{Z_i} and $n_{Z_{q,sca}}$ are independent and have variance $N_0/(2T)$. It will be shown in Section IV that the inphase and quadrature signals of the BTD suppressed carrier loop have the same statistics as are found in Eqs. (11) and (12). Hence, both suppressed carrier loops will have the same error signal and tracking performance.

III. Baseband Recording

As indicated earlier, the BTD processes the received signal after the signal has been open-loop downconverted to baseband on a subcarrier harmonic basis and recorded on tape. This section describes two methods for recording the received signal at baseband. The first recording scheme, depicted in Fig. 2, distributes the sampled IF signal into two carrier channels and $4n$ subcarrier channels, where n denotes the number of subcarrier harmonics present at the A/D output and is related to L (the highest recorded subcarrier harmonic) through $L = 2n - 1$. Recording of the carrier requires two channels because baseband demodulation requires both inphase and quadrature samples. Similarly, recording of each subcarrier harmonic requires four channels—two channels (one inphase subcarrier channel and one quadrature subcarrier channel) per carrier channel (inphase and quadrature). Table 1 depicts the loss in data power as a function of the highest recorded subcarrier harmonic L.

Each band of the sampled IF signal is recorded at baseband after mixing it with tones tuned to its predicted center frequency. The predicts are assumed to be close, but not exactly equal, to the actual band center frequency. For example, consider the two channels that record the residual carrier. In the residual carrier sine channel, the sampled IF signal is mixed with $\sqrt{2}\sin\hat{\Psi}_c(kT_s)$, where $\hat{\Psi}_c(kT_s)$ is an estimate of the actual carrier phase $\Psi_c(kT_s)$, and is lowpass filtered to obtain the recorded waveform $C_s(kT_s)$. Similarly, in the residual carrier cosine channel, the sampled IF signal is mixed with $\sqrt{2}\cos\hat{\Psi}_c(kT_s)$ and lowpass filtered to obtain $C_c(kT_s)$. Given the information in Appendix A, let $\Theta_c(kT_s) \triangleq \Psi_c(kT_s) - \hat{\Psi}_c(kT_s)$, the recorded carrier is given by

$$C_s = \sqrt{P_c}\cos(\Theta_c) + n_{c_s} \tag{13}$$

$$C_c = \sqrt{P_c}\sin(\Theta_c) + n_{c_c} \tag{14}$$

where, using the Heaviside operator notation,[1]

$$n_{c_s} = H_c(z)\{-n_1\sin(\Theta_c) - n_2\cos(\Theta_c)\} \tag{15}$$

$$n_{c_c} = H_c(z)\{n_1\cos(\Theta_c) - n_2\sin(\Theta_c)\} \tag{16}$$

The lowpass filter $H_c(z)$ is assumed to be bandlimited to B_c Hz. Furthermore, since the carrier frequency error (derivative of Θ_c) is assumed to be much smaller than B_c, both n_{c_c} and n_{c_s} are baseband processes limited to B_c and have a flat, one-sided PSD level equal to N_0 W/Hz.

In the first approach, the recording of the subcarrier harmonics at baseband requires a two-stage downconversion of the IF signal. The first stage centers the IF spectrum near DC by mixing it with sine and cosine references tuned to the predicted carrier frequency. The second stage mixes each of the subcarrier harmonics to baseband individually by mixing the output of the first stage with sine and cosine references tuned to multiples of the predicted subcarrier frequency. Hence, to record the mth subcarrier harmonic, the IF signal is first mixed with $\sin(\hat{\Psi}_c)$ and $\cos(\hat{\Psi}_c)$, and then with $\sin(m\hat{\Psi}_{su})$ and $\cos(m\hat{\Psi}_{su})$. It is important to note that a phase relationship has to be maintained between the various tones that demodulate the subcarrier harmonics to baseband. Given the information in Appendix A, the four signals corresponding to the recording of the mth subcarrier harmonic are represented as (where m is an odd integer)

$$SU_{ss}^{(m)} = -\sqrt{P_d}\frac{2d}{\pi m}\cos[m\Theta_{su}]\sin(\Theta_c) + n_{SU_{ss}}^{(m)} \tag{17}$$

[1] The Heaviside operation $H(z)\{x(m)\} \triangleq \sum_{n=-\infty}^{m} x(n)h(m-n)$ denotes the convolution of $x(m)$ with $h(m)$.

$$SU_{sc}^{(m)} = -\sqrt{P_d}\frac{2d}{\pi m}\sin[m\Theta_{su}]\sin(\Theta_c) + n_{SU_{sc}}^{(m)} \quad (18)$$

$$SU_{cs}^{(m)} = +\sqrt{P_d}\frac{2d}{\pi m}\cos[m\Theta_{su}]\cos(\Theta_c) + n_{SU_{cs}}^{(m)} \quad (19)$$

$$SU_{cc}^{(m)} = +\sqrt{P_d}\frac{2d}{\pi m}\sin[m\Theta_{su}]\cos(\Theta_c) + n_{SU_{cc}}^{(m)} \quad (20)$$

where the noise terms are given by

$$n_{SU_{ss}}^{(m)} = -H_{su}(z)\left\{[n_1\sin(\Theta_c) + n_2\cos(\Theta_c)]\sin[m\hat{\Psi}_{su}]\right\} \quad (21)$$

$$n_{SU_{sc}}^{(m)} = -H_{su}(z)\left\{[n_1\sin(\Theta_c) + n_2\cos(\Theta_c)]\cos[m\hat{\Psi}_{su}]\right\} \quad (22)$$

$$n_{SU_{cs}}^{(m)} = H_{su}(z)\left\{[n_1\cos(\Theta_c) - n_2\sin(\Theta_c)]\sin[m\hat{\Psi}_{su}]\right\} \quad (23)$$

$$n_{SU_{cc}}^{(m)} = H_{su}(z)\left\{[n_1\cos(\Theta_c) - n_2\sin(\Theta_c)]\cos[m\hat{\Psi}_{su}]\right\} \quad (24)$$

It can be verified that $n_{SU_{sc}}^{(m)}$, $n_{SU_{ss}}^{(m)}$, $n_{SU_{cc}}^{(m)}$, and $n_{SU_{cs}}^{(m)}$ are baseband processes limited to B_{su}, the bandwidth of the lowpass filter $H_{su}(z)$, and have a flat, one-sided PSD level equal to $N_0/2$ W/Hz. Moreover, it can be shown that these recorded noises are not only mutually independent of each other for every subcarrier harmonic (say, m), but are also independent of the recorded noises at other harmonics (any $n \neq m$).

Another approach to baseband recording of the received signal is shown in Fig. 3. Unlike the previous recording scheme, which uses the two-stage downconversion technique to record the subcarrier, this scheme records each subcarrier harmonic by directly downconverting it to baseband. As shown in Fig. 3, the sampled IF signal is still distributed into $(4n+2)$ channels. The two channels used for recording the residual carrier remain the same for this new scheme. Consequently, the recorded carrier is as given by Eqs. (13) and (14). However, the subcarrier harmonics are recorded at baseband by directly mixing the upper and lower sidebands of each harmonic to baseband. That is, the mth subcarrier harmonic is recorded after mixing the A/D output with sine and cosine references tuned to $\hat{f}_c + m\hat{f}_{su}$ (upper sideband) and $\hat{f}_c - m\hat{f}_{su}$ (lower sideband) where $\hat{f}_c$ and $\hat{f}_{su}$ denote, respectively, the predicted carrier and subcarrier frequencies. Following the same procedure used in the derivation of Eqs. (17)–(20) (see Appendix A), the recorded signals for this scheme can be shown to be (where m is an odd integer)

$$SU_{s+}^{(m)} = \sqrt{P_d}\frac{2d}{\pi m}\cos[\Theta_c + m\Theta_{su}] + n_{SU_{s+}}^{(m)} \quad (25)$$

$$SU_{s-}^{(m)} = -\sqrt{P_d}\frac{2d}{\pi m}\cos[\Theta_c - m\Theta_{su}] + n_{SU_{s-}}^{(m)} \quad (26)$$

$$SU_{c+}^{(m)} = \sqrt{P_d}\frac{2d}{\pi m}\sin[\Theta_c + m\Theta_{su}] + n_{SU_{c+}}^{(m)} \quad (27)$$

$$SU_{c-}^{(m)} = -\sqrt{P_d}\frac{2d}{\pi m}\sin[\Theta_c - m\Theta_{su}] + n_{SU_{c-}}^{(m)} \quad (28)$$

where the subscripts "+" and "−", respectively, denote the upper and lower sidebands. The noises $n_{SU_{s+}}^{(m)}$, $n_{SU_{s-}}^{(m)}$, $n_{SU_{c+}}^{(m)}$, and $n_{SU_{s+}}^{(m)}$ can be shown to have a flat, one-sided PSD level equal to N_0 within B_{su} Hz, the one-sided bandwidth of the lowpass filter $H_{su}(z)$ in Fig. 3. These upper and lower sideband noises are correlated with respect to each other because the recorded signals of the direct recording scheme are correlated. Specifically, they are related to each other by Eqs. (17)–(20) as follows; namely,

$$SU_{s+}^{(m)} = SU_{sc}^{(m)} + SU_{cs}^{(m)} \quad (29)$$

$$SU_{s-}^{(m)} = SU_{sc}^{(m)} - SU_{cs}^{(m)} \quad (30)$$

$$SU_{c+}^{(m)} = SU_{cc}^{(m)} - SU_{ss}^{(m)} \quad (31)$$

$$SU_{c-}^{(m)} = SU_{cc}^{(m)} + SU_{ss}^{(m)} \quad (32)$$

and consequently,

$$n_{SU_{s+}}^{(m)} = n_{SU_{sc}}^{(m)} + n_{SU_{cs}}^{(m)} \quad (33)$$

$$n_{SU_{s-}}^{(m)} = n_{SU_{sc}}^{(m)} - n_{SU_{cs}}^{(m)} \quad (34)$$

$$n_{SU_{c+}}^{(m)} = n_{SU_{cc}}^{(m)} - n_{SU_{ss}}^{(m)} \quad (35)$$

$$n_{SU_{c-}}^{(m)} = n_{SU_{cc}}^{(m)} + n_{SU_{ss}}^{(m)} \quad (36)$$

Clearly, $n_{SU_{s+}}^{(m)}$ is correlated with $n_{SU_{s-}}^{(m)}$ and $n_{SU_{c+}}^{(m)}$ is correlated with $n_{SU_{c-}}^{(m)}$.

IV. Coherent Baseband Demodulation

This section considers the coherent baseband demodulation of the carrier and subcarrier when the modulation index (Δ in Eq. [1]) is such that the received signal consists of a sinusoidal carrier and square-wave subcarrier; it also considers the case when the received signal consists of a suppressed carrier with square-wave subcarrier (i.e., $\Delta = 90$ deg). The demodulation functions begin by reading the recorded signals of Section III from a tape drive and then processing them to obtain control signals for the carrier, subcarrier, and suppressed carrier tracking loops. Recall that two methods for baseband recording of the IF signal were considered in Section III. It will be shown that the baseband processing corresponding to these two methods is very similar except for a little extra processing that is required for the direct downconversion scheme, the second recording scheme in Section III. In this section, the carrier tracking loop, which is the same for both recording schemes, is described first. Then, the subcarrier and suppressed carrier loops for the two-stage downconversion recording scheme are described, and followed by the additional processing needed for using the signals of the direct downconversion scheme.

The carrier tracking loop, depicted near the bottom of Fig. 4, mixes the signals C_c and C_s with $\cos(\hat{\Theta}_c)$ and $\sin(\hat{\Theta}_c)$, respectively, before subtracting the mixer outputs and accumulating the resulting samples over the loop update interval to form the carrier loop control signal, V_q. Hence,

$$V_q = \frac{1}{M_1} \sum_{M_1} [C_c \cos(\hat{\Theta}_c) - C_s \sin(\hat{\Theta}_c)] \quad (37)$$

where $\hat{\Theta}_c$ is an estimate of the recorded carrier phase Θ_c. Substituting Eqs. (13) and (14) for C_s and C_c, then expanding and canceling common terms, and assuming that the carrier phase error, $\phi_c \triangleq \Theta_c - \hat{\Theta}_c$, varies slowly over the loop update interval, $T_u = M_1 T_s$, yields

$$V_q = \sqrt{P_c} \sin(\phi_c) + n_{V_q} \quad (38)$$

where

$$n_{V_q} = \frac{1}{M_1} \sum_{M_1} [n_{cc} \cos(\hat{\Theta}_c) - n_{cs} \sin(\hat{\Theta}_c)] \quad (39)$$

and n_{cs} and n_{cc} are given by Eqs. (15) and (16). Since both n_{cs} and n_{cc} are zero mean with a flat, one-sided power spectral density level equal to N_0 W/Hz within a much wider recording bandwidth B_c than the loop update rate $1/T_u$ has, it can be shown that n_{V_q} is Gaussian with zero mean and variance $N_0/2T_u$. Comparing Eq. (38) with Eq. (6) indicates that both the baseband carrier loop and the IF carrier loop have the same control signal in terms of signal power and noise variance. As a result, the carrier tracking variance of the baseband loop will be the same as that of a phase-locked loop tuned to the intermediate frequency.

Recall that the square-wave subcarrier was recorded at baseband by mixing each of its harmonics down to baseband individually and then recording each harmonic separately. For each subcarrier harmonic retained, four baseband signals given by Eqs. (17) through (20) were actually recorded. As shown in Fig. 4, each harmonic of the subcarrier is first read from the tape recorder and demodulated individually, and then properly weighted and summed to reconstruct the proper inphase and quadrature samples for the various Costas loops. The demodulation procedures require that the four recorded signals of each subcarrier harmonic be multiplied by the estimated carrier references, $\sin(\hat{\Theta}_c)$ and $\cos(\hat{\Theta}_c)$, and the estimated subcarrier harmonic references, $\sin(m\hat{\Theta}_c)$ and $\cos(m\hat{\Theta}_c)$, where m is an odd integer that depends on the subcarrier harmonic under consideration. As depicted in Fig. 4, the resulting signals are either added or subtracted to retain terms at $\Theta_c - \hat{\Theta}_c$ and $m(\Theta_{su} - \hat{\Theta}_{su})$, and eliminate terms at $\Theta_c + \hat{\Theta}_c$ and $m(\Theta_{su} + \hat{\Theta}_{su})$. The details of these demodulation procedures are provided in Appendix A. Each of the demodulated signals of a particular subcarrier harmonic is then properly weighted and summed to reconstruct the desired control signals for various tracking loops. For example, in the subcarrier loop depicted in the top half of Fig. 4, the mth harmonic is scaled by $4/(m\pi)$ on the inphase arm, and $[4/(m\pi)] \sin[(m/2)\pi W_{su}]$ on the quadrature arm (W_{su} is the subcarrier window size). Subsequently, the scaled inphase signals corresponding to each harmonic are added to form the input to the inphase symbol accumulator, whereas the scaled quadrature signals are added to form the input to the quadrature symbol accumulator. The product of the inphase accumulator output, Y_i in Fig. 4, and the quadrature accumulator output, $Y_{q,su}$ in Fig. 4, is the subcarrier loop control signal. Given the information in Appendix A, the symbol accumulator outputs corresponding to the lth symbol are given as

$$Y_i = \sqrt{P_d} a_l \cos(\phi_c) \frac{8}{\pi^2} \sum_{\substack{j=1 \\ j:odd}}^{L} \left(\frac{1}{j^2} \cos(j\phi_{su}) \right) + n_{Y_i} \quad (40)$$

and

$$Y_{q,su} = \sqrt{P_d} a_l \cos(\phi_c) \frac{8}{\pi^2} \sum_{\substack{j=1 \\ j:odd}}^{L} \left(\frac{\sin[(j/2)\pi W_{su}]}{j^2} \sin(j\phi_{su}) \right)$$

$$+ n_{Y_{q,su}} \quad (41)$$

where the independent noise terms, n_{Y_i} and $n_{Y_{q,su}}$, are shown in Appendix A to have variance $N_0/(2T)$ and $N_0 W_{su}/(2T)$, respectively, as L approaches infinity in the above two equations. That is, for sufficiently large L, the noise variances of n_{Y_i} and $n_{Y_{q,su}}$ are approximately the same as the variances of n_{Z_i} and $n_{Z_{q,su}}$ in Eqs. (7) and (8), respectively. Furthermore, the signal parts of Eqs. (40) and (7), and of Eqs. (41) and (8), are also equal as L approaches infinity. This can be easily shown by using the Fourier series expansion of $F_I(\phi_{su})$ and $F_Q(\phi_{su})$ in Eqs. (7) and (8), given as follows:

$$F_I(\phi_{su}) = \frac{8}{\pi^2} \sum_{\substack{j=1 \\ j:odd}}^{\infty} \frac{1}{j^2} \cos(j\phi_{su}) \quad (42)$$

and

$$F_Q(\phi_{su}) = \frac{8}{\pi^2} \sum_{\substack{j=1 \\ j:odd}}^{\infty} \frac{\sin[(j/2)\pi W_{su}]}{j^2} \sin(j\phi_{su}) \quad (43)$$

As a result of the subcarrier loop accumulator outputs of the ARX II and BTD being approximately equal for sufficiently large L, the control signals, $Y_i Y_{q,su}$ and $Z_i Z_{q,su}$, and tracking variance of both loops can also be shown to be equal.

For suppressed carrier tracking, the suppressed carrier loop, also shown in Fig. 4, is a Costas loop sharing the same inphase arm with the subcarrier Costas loop. Hence, the suppressed carrier inphase accumulator output, Y_i, is as given in Eq. (40). The processing in the suppressed carrier loop quadrature arm is very similar to that of the subcarrier loop. Hence, following the same derivation as in the subcarrier loop quadrature arm, the suppressed carrier quadrature arm accumulation over the lth symbol can be shown to be

$$Y_{q,sca} = \sqrt{P_d} a_l \sin(\phi_c) \frac{8}{\pi^2} \sum_{\substack{j=1 \\ j:odd}}^{L} \frac{1}{j^2} \cos(j\phi_{su}) + n_{Y_{q,sca}} \quad (44)$$

As before, the equivalence of the suppressed carrier loops of the BTD and ARX II is established by comparing the inphase and quadrature accumulator outputs of both loops. The equivalence of the inphase arms has already been shown earlier. The signal parts of the quadrature arm accumulations given by Eqs. (12) and (44) are seen to be equivalent after letting L go to infinity in Eq. (44) and then using Eq. (42) for the infinite sum. The noise parts of Eqs. (12) and (44), as L approaches infinity in Eq. (44), can also be shown to have the same variance $(N_0/2T)$. Furthermore, it can be shown that n_{Y_i} and $n_{Y_{q,sca}}$ are uncorrelated.

Finally, consider the coherent baseband demodulation of the signals that were recorded as a result of the direct downconversion scheme, the second recording scheme described in Section III. As indicated earlier, the demodulator for the direct scheme is very similar to the two-stage downconversion scheme demodulator except that the former requires a little extra processing. Specifically, the recorded signals for the direct scheme, given by Eqs. (25)-(28), are combined to yield the signals $SU_{ss}^{(m)}$, $SU_{sc}^{(m)}$, $SU_{cs}^{(m)}$, and $SU_{cc}^{(m)}$, which were the input signals to the two-stage demodulator described in this section. From Eqs. (29)-(32), it is clear that the input signals to the two-stage demodulator can be generated by using two adders and two subtractors (per harmonic) on the signals $SU_{s+}^{(m)}$, $SU_{s-}^{(m)}$, $SU_{c+}^{(m)}$, and $SU_{c-}^{(m)}$. After these additions and subtractions, shown in Fig. 5, the rest of the signal processing remains the same as in the previous scheme.

V. Requirements for Software Implementation of the BTD

As indicated earlier, the BTD depicted in Fig. 4 is targeted for implementation on a general-purpose engineering workstation. The primary concern with a software implementation is whether a general-purpose workstation can provide the computational speed required for real-time processing of the recorded signals. For example, if the received symbol rate is 1K symbols/sec and the A/D sampling rate is 10K samples/sec, then a real-time demodulator would process 10K samples/sec and detect 1K symbols/sec. This section first determines the computational speed required (in operations/sec) for implementing the BTD in real time when the symbol rate is 1K symbols/sec and the sample rate is 10K samples/sec. Next, it deter-

mines the feasibility of implementing the BTD on a Sun Sparc 2 (SS-2) and Sun Sparc 10 workstation.

Recall that the two modes for the BTD are the residual carrier with subcarrier mode ($\Delta \neq 90$ deg) and the suppressed carrier with subcarrier mode ($\Delta = 90$ deg). The number of (addition and multiplication) operations/sec, for a given mode, can be computed by separately counting the operations/sample and operations/symbol in Fig. 4 and then multiplying by the operations at the sampling rate and the operations at the symbol rate. Mathematically,

$$\text{operations} = \left(\frac{(\text{number of "+" and "}\times\text{"}) \text{ operations}}{\text{sample}}\right) \times \left(\frac{\text{10K samples}}{\text{sec}}\right) + \left(\frac{(\text{number of "+" and "}\times\text{"}) \text{ operations}}{\text{symbol}}\right) \times \left(\frac{\text{1K symbols}}{\text{sec}}\right) \quad (45)$$

where the sample and symbol (floating point) operations for the coherent demodulator in Fig. 4 are tabulated in Table 2(a). The total number of operations in Table 2(a) is accounted for in more detail in Table 2(b). The coherent demodulator for the direct downconversion scheme needs four more sample operations per harmonic than that of the two-stage downconversion scheme, as shown in Fig. 5, and is not considered separately. Note that both addition and multiplication are counted as one operation each. Furthermore, the lookup table operations are done at the 10K samples/sec rate, since the lookup table is considered to be part of the carrier and subcarrier numerically controlled oscillators (NCO's). With the number of harmonics, n, equal to three (i.e., the first, third, and fifth harmonics are recorded) in Table 2(a), there are 71 operations/sample and 38 operations/symbol for the residual carrier mode, and there are 98 operations/sample and 39 operations/symbol in the suppressed carrier mode. Consequently, at 1K samples/sec and 10 KHz sampling rate, a real-time processor would be required to provide 748K and 1019K operations for the residual carrier and suppressed carrier modes, respectively. The number of operations per second and the SNR degradation as a function of subcarrier harmonics are tabulated in Table 2(b). Table 3 lists the throughput utilized by a software implementation of the BTD for various computers. The throughput is defined as the number of instructions a computer can execute per second. In Table 3, the percentage of throughput utilized by a Sun SS-2 was obtained by simulating a portion of the BTD on the Sun SS-2 and then linearly extrapolating the results to determine the throughput utilization for a software implementation of the entire BTD. The throughput of the remaining computers was obtained by linearly extrapolating the Sun SS-2 results using the SPECfp92 benchmark. The specmark rating of a computer, obtained by running a collection of commonly used programs on a target system, is a measure of the computer's performance relative to a VAX-11/780. For example, the Sun SS-2 is expected to perform 22.8 times better than a VAX-11/780, since it specmarks at 22.8. Alternatively stated, the throughput utilization of the Sun SS-2 is expected to be (1/22.8) that of a VAX-11/780. It is clear from Table 3 that several computers will be able to process the recorded data in real time.

References

[1] S. Hinedi, "A Functional Description of the Advanced Receiver," *The Telecommunications and Data Acquisition Progress Report 42-100*, vol. October–December 1989, Jet Propulsion Laboratory, Pasadena, California, pp. 131–149, February 15, 1990.

[2] J. H. Yuen, *Deep Space Telecommunications Systems Engineering*, New York: Plenum Press, 1983.

[3] W. J. Hurd and S. Aguirre, "A Method to Dramatically Improve Subcarrier Tracking," *The Telecommunications and Data Acquisition Progress Report 42-86*, vol. April–June 1986, Jet Propulsion Laboratory, Pasadena, California, pp. 103–110, August 15, 1986.

Glossary

Ψ_c = Incoming carrier phase

$\hat{\Psi}_c$ = Predicted carrier phase

Θ_c = Carrier phase offset, $\Psi_c - \hat{\Psi}_c$

$\hat{\Theta}_c$ = Carrier phase offset estimate

ϕ_c = Carrier phase offset error, $\Theta_c - \hat{\Theta}_c$

Ψ_{su} = Incoming subcarrier phase

$\hat{\Psi}_{su}$ = Predicted subcarrier phase

Θ_{su} = Subcarrier phase offset, $\Psi_{su} - \hat{\Psi}_{su}$

$\hat{\Theta}_{su}$ = Subcarrier phase offset estimate

ϕ_{su} = Subcarrier phase offset error, $\Theta_{su} - \hat{\Theta}_{su}$

$XSU_{ss}^{(m)}$ = mth subcarrier harmonic, derived from mixing the received signal with $\sqrt{2}\sin(\hat{\Psi}_c)\sin(m\hat{\Psi}_{su})$

$SU_{ss}^{(m)}$ = The lowpass filtered version of $XSU_{ss}^{(m)}$

$XSU_{sc}^{(m)}$ = mth subcarrier harmonic, derived from mixing the received signal with $\sqrt{2}\sin(\hat{\Psi}_c)\cos(m\hat{\Psi}_{su})$

$SU_{sc}^{(m)}$ = The lowpass filtered version of $XSU_{sc}^{(m)}$

$XSU_{cs}^{(m)}$ = mth subcarrier harmonic, derived from mixing the received signal with $\sqrt{2}\cos(\hat{\Psi}_c)\sin(m\hat{\Psi}_{su})$

$SU_{cs}^{(m)}$ = The lowpass filtered version of $XSU_{cs}^{(m)}$

$XSU_{cc}^{(m)}$ = mth subcarrier harmonic, derived from mixing the received signal with $\sqrt{2}\cos(\hat{\Psi}_c)\cos(m\hat{\Psi}_{su})$

$SU_{cc}^{(m)}$ = The lowpass filtered version of $XSU_{cc}^{(m)}$

$XSU_{s+}^{(m)}$ = mth subcarrier harmonic, derived from mixing the received signal with $\sqrt{2}\sin(\hat{\Psi}_c + m\hat{\Psi}_{su})$

$SU_{s+}^{(m)}$ = The lowpass filtered version of $XSU_{s+}^{(m)}$

$XSU_{s-}^{(m)}$ = mth subcarrier harmonic, derived from mixing the received signal with $\sqrt{2}\sin(\hat{\Psi}_c - m\hat{\Psi}_{su})$

$SU_{s-}^{(m)}$ = The lowpass filtered version of $XSU_{s-}^{(m)}$

$XSU_{c+}^{(m)}$ = mth subcarrier harmonic, derived from mixing the received signal with $\sqrt{2}\cos(\hat{\Psi}_c + m\hat{\Psi}_{su})$

$SU_{c+}^{(m)}$ = The lowpass filtered version of $XSU_{c+}^{(m)}$

$XSU_{c-}^{(m)}$ = mth subcarrier harmonic, derived from mixing the received signal with $\sqrt{2}\cos(\hat{\Psi}_c - m\hat{\Psi}_{su})$

$SU_{c-}^{(m)}$ = The lowpass filtered version of $XSU_{c-}^{(m)}$

Appendix A

I. Derivation of Eqs. (13) and (14)

As shown in Fig. 2, the lowpass filter inputs XC_s and XC_c are given as

$$XC_s = r\sqrt{2}\sin(\hat{\Psi}_c) \tag{A-1}$$

$$XC_c = r\sqrt{2}\cos(\hat{\Psi}_c) \tag{A-2}$$

where the digitized IF, r, is given by Eq. (4) and $\hat{\Psi}_c$ is the predicted carrier phase. (The index kT_s is omitted for simplicity of notation.) Substituting Eq. (4) into Eqs. (A-1) and (A-2), then expanding and letting $\Theta_c = \Psi_c - \hat{\Psi}_c$, yields

$$XC_s = \sqrt{P_c}\cos(\Theta_c) - n_1\sin(\Theta_c) - n_2\cos(\Theta_c) - \sqrt{P_d}d\left(\frac{4}{\pi}\sum_{\substack{j=1\\ j:odd}}^{L}\frac{1}{j}\sin[j\Psi_{su}]\right)\sin(\Theta_c)$$

$$+ \left(\text{terms at angular frequency } (\Psi_c + \hat{\Psi}_c)'\right) \tag{A-3}$$

and

$$XC_c = \sqrt{P_c}\sin(\Theta_c) + n_1\cos(\Theta_c) - n_2\sin(\Theta_c) + \sqrt{P_d}d\left(\frac{4}{\pi}\sum_{\substack{j=1\\ j:odd}}^{L}\frac{1}{j}\sin[j\Psi_{su}]\right)\cos(\Theta_c)$$

$$+ \left(\text{terms at angular frequency } (\Psi_c + \hat{\Psi}_c)'\right) \tag{A-4}$$

where the instantaneous angular frequency (in radians/sec) of the high-frequency components is denoted as $(\Psi_c + \hat{\Psi}_c)'$, the time derivative of the total phase $\Psi_c + \hat{\Psi}_c$.

From Eqs. (A-3) and (A-4), it is clear that XC_s and XC_c have the desired baseband carrier at angular frequency, Θ_c'—as well as the undesired data spectra centered at $\Theta_c' \pm j\Psi_{su}'$, where Ψ_{su}' is the angular subcarrier frequency and j is an odd integer, $1 \le j \le L$—and other undesired terms at frequency $(\Psi_c + \hat{\Psi}_c)'$. The recorded baseband carrier given by Eqs. (13) and (14) can be obtained by lowpass filtering XC_s and XC_c with the filter $H_c(z)$ whose bandwidth B_c is small enough to accommodate only the desired baseband carrier, i.e.,

$$B_c \le (-\Theta_c' + \Psi_{su}' - \omega_d)/(2\pi) \quad \text{(in Hz)}$$

where ω_d is the bandwidth (in radians/sec) wherein most of the data power resides.

II. Derivation of Eqs. (17) Through (20)

As shown in Fig. 2, recording of the mth harmonic of the data-modulated subcarrier requires downconverting this particular harmonic to baseband by mixing XC_s and XC_c with both the inphase and quadrature subcarrier references tuned to the predicted frequency of the mth harmonic. Here, m is an odd integer with $1 \leq m \leq L$, where L is the highest subcarrier harmonic to be recorded. The four signals that are generated as a result are as follows:

$$XSU_{ss}^{(m)} = XC_s \sin(m\hat{\Psi}_{su}) \tag{A-5}$$

$$XSU_{sc}^{(m)} = XC_s \cos(m\hat{\Psi}_{su}) \tag{A-6}$$

$$XSU_{cs}^{(m)} = XC_c \sin(m\hat{\Psi}_{su}) \tag{A-7}$$

$$XSU_{cc}^{(m)} = XC_c \cos(m\hat{\Psi}_{su}) \tag{A-8}$$

It can be found that (with $\Theta_{su} = \Psi_{su} - \hat{\Psi}_{su}$)

$$\begin{aligned} XSU_{ss}^{(m)} &= \sqrt{P_c}\cos(\Theta_c)\sin(m\hat{\Psi}_{su}) - \sqrt{P_d}\frac{2d}{m\pi}\sin(\Theta_c)\cos(m\Theta_{su}) \\ &\quad - \sqrt{P_d}\frac{2d}{\pi}\sin(\Theta_c)\left(\sum_{\substack{j=1 \\ j:odd,\ j\neq m}}^{L}\frac{1}{j}\cos\left(j\Psi_{su} - m\hat{\Psi}_{su}\right)\right) - [n_1\sin(\Theta_c) + n_2\cos(\Theta_c)]\sin(m\hat{\Psi}_{su}) \\ &\quad + \left(\text{terms at angular frequency } (\Psi_c + \hat{\Psi}_c)'\right) \end{aligned} \tag{A-9}$$

$$\begin{aligned} XSU_{sc}^{(m)} &= \sqrt{P_c}\cos(\Theta_c)\cos(m\hat{\Psi}_{su}) - \sqrt{P_d}\frac{2d}{m\pi}\sin(\Theta_c)\sin(m\Theta_{su}) \\ &\quad - \sqrt{P_d}\frac{2d}{\pi}\sin(\Theta_c)\left(\sum_{\substack{j=1 \\ j:odd,\ j\neq m}}^{L}\frac{1}{j}\sin\left(j\Psi_{su} - m\hat{\Psi}_{su}\right)\right) - [n_1\sin(\Theta_c) + n_2\cos(\Theta_c)]\cos(m\hat{\Psi}_{su}) \\ &\quad + \left(\text{terms at angular frequency } (\Psi_c + \hat{\Psi}_c)'\right) \end{aligned} \tag{A-10}$$

$$\begin{aligned} XSU_{cs}^{(m)} &= \sqrt{P_c}\sin(\Theta_c)\sin(m\hat{\Psi}_{su}) + \sqrt{P_d}\frac{2d}{m\pi}\cos(\Theta_c)\cos(m\Theta_{su}) \\ &\quad + \sqrt{P_d}\frac{2d}{\pi}\cos(\Theta_c)\left(\sum_{\substack{j=1 \\ j:odd,\ j\neq m}}^{L}\frac{1}{j}\cos\left(j\Psi_{su} - m\hat{\Psi}_{su}\right)\right) + [n_1\cos(\Theta_c) - n_2\sin(\Theta_c)]\sin(m\hat{\Psi}_{su}) \\ &\quad + \left(\text{terms at angular frequency } (\Psi_c + \hat{\Psi}_c)'\right) \end{aligned} \tag{A-11}$$

$$XSU_{cc}^{(m)} = \sqrt{P_c}\sin(\Theta_c)\cos(m\hat{\Psi}_{su}) + \sqrt{P_d}\frac{2d}{m\pi}\cos(\Theta_c)\sin(m\Theta_{su})$$

$$+ \sqrt{P_d}\frac{2d}{\pi}\cos(\Theta_c)\left(\sum_{\substack{j=1 \\ j:odd,\ j\neq m}}^{L}\frac{1}{j}\sin\left(j\Psi_{su} - m\hat{\Psi}_{su}\right)\right) + [n_1\cos(\Theta_c) - n_2\sin(\Theta_c)]\cos(m\hat{\Psi}_{su})$$

$$+ \left(\text{terms at angular frequency } (\Psi_c + \hat{\Psi}_c)'\right) \qquad \text{(A-12)}$$

It is clear that the baseband signal component in each of $XSU_{ss}^{(m)}$, $XSU_{sc}^{(m)}$, $XSU_{cs}^{(m)}$, and $XSU_{cc}^{(m)}$ is represented by the second term in each of the above four equations, since the subcarrier frequency error, denoted by Θ'_{su}, is assumed to be very close to zero. The recorded mth subcarrier harmonic signals given in Eqs. (17) to (20) for any odd integer $1 \leq m \leq L$ are the corresponding baseband components in Eqs. (A-9) to (A-12). These signals can be extracted by lowpass filtering $XSU_{ss}^{(m)}$, $XSU_{sc}^{(m)}$, $XSU_{cs}^{(m)}$, and $XSU_{cc}^{(m)}$ with the filter $H_{su}(z)$, of which the bandwidth B_{su} is wide enough to accommodate both the carrier frequency offset and the maximum subcarrier frequency offsets (up to the highest subcarrier harmonic recorded) as well as the data modulation, namely,

$$B_{su} \geq (\Theta'_c + L\Theta'_{su} + \omega_d)/(2\pi) \quad \text{(in Hz)}$$

where ω_d is the bandwidth (in radians/sec) wherein most of the data power resides.

III. Derivation of Eqs. (40) and (41)

In referring to the subcarrier loop in Fig. 4, it is seen that the mth subcarrier harmonic waveforms $SU_{sc}^{(m)}$, $SU_{ss}^{(m)}$, $SU_{cc}^{(m)}$, and $SU_{cs}^{(m)}$ are demodulated as follows:

$$A^{(m)} = SU_{cs}^{(m)}\cos(\hat{\Theta}_c) - SU_{ss}^{(m)}\sin(\hat{\Theta}_c) \qquad \text{(A-13)}$$

$$B^{(m)} = SU_{cc}^{(m)}\cos(\hat{\Theta}_c) - SU_{sc}^{(m)}\sin(\hat{\Theta}_c) \qquad \text{(A-14)}$$

where the references $\sin(\hat{\Theta}_c)$ and $\cos(\hat{\Theta}_c)$ have the estimated carrier error phase $\hat{\Theta}_c$ obtained from the carrier tracking. It can be found that

$$A^{(m)} = \sqrt{P_d}\frac{2d}{m\pi}\cos(m\Theta_{su})\cos(\phi_c) + n_A^{(m)} \qquad \text{(A-15)}$$

$$B^{(m)} = \sqrt{P_d}\frac{2d}{m\pi}\sin(m\Theta_{su})\cos(\phi_c) + n_B^{(m)} \qquad \text{(A-16)}$$

where

$$n_A^{(m)} = n_{SUcs}^{(m)}\cos(\hat{\Theta}_c) - n_{SUss}^{(m)}\sin(\hat{\Theta}_c) \qquad \text{(A-17)}$$

$$n_B^{(m)} = n_{SUcc}^{(m)}\cos(\hat{\Theta}_c) - n_{SUsc}^{(m)}\sin(\hat{\Theta}_c) \qquad \text{(A-18)}$$

It is clear that both $n_A^{(m)}$ and $n_B^{(m)}$ have a flat, one-sided PSD level equal to $N_0/2$ W/Hz within the frequency interval $[0, B_{su}]$ Hz, since $n_{SUss}^{(m)}$, $n_{SUsc}^{(m)}$, $n_{SUcs}^{(m)}$, and $n_{SUcc}^{(m)}$ have the same PSD level ($N_0/2$, one-sided) within the same bandwidth (B_{su}). Note that B_{su} is the bandwidth of the filter $H_{su}(z)$ in Fig. 2. Furthermore, it can be shown that both $n_A^{(m)}$ and $n_B^{(m)}$ are not only independent of each other, but also independent of their counterparts at other subcarrier harmonics.

The signals $A^{(m)}$ and $B^{(m)}$ are multiplied by the subcarrier references and then added or subtracted, as shown in Fig. 4, to remove the subcarrier frequency error. The resulting signals, $X_i^{(m)}$ and $X_{q,su}^{(m)}$, are given as follows:

$$X_i^{(m)} = A^{(m)}\cos(m\hat{\Theta}_{su}) + B^{(m)}\sin(m\hat{\Theta}_{su}) \qquad \text{(A-19)}$$

$$X_{q,su}^{(m)} = B^{(m)}\cos(m\hat{\Theta}_{su}) - A^{(m)}\sin(m\hat{\Theta}_{su}) \qquad \text{(A-20)}$$

Substituting the expressions for $A^{(m)}$ and $B^{(m)}$, then letting $\phi_c = \Theta_c - \hat{\Theta}_c$ and $\phi_{su} = \Theta_{su} - \hat{\Theta}_{su}$, yields

$$X_i^{(m)} = \sqrt{P_d}\frac{2d}{m\pi}\cos(m\phi_{su})\cos(\phi_c) + n_{X_i}^{(m)} \qquad \text{(A-21)}$$

$$X_{q,su}^{(m)} = \sqrt{P_d}\frac{2d}{m\pi}\sin(m\phi_{su})\cos(\phi_c) + n_{X_{q,su}}^{(m)} \qquad \text{(A-22)}$$

where

$$n_{X_i}^{(m)} = n_A^{(m)} \cos(m\hat{\Theta}_{su}) + n_B^{(m)} \sin(m\hat{\Theta}_{su}) \quad \text{(A-23)}$$

$$n_{X_{q,su}}^{(m)} = n_B^{(m)} \cos(m\hat{\Theta}_{su}) - n_A^{(m)} \sin(m\hat{\Theta}_{su}) \quad \text{(A-24)}$$

In referring to the weighted summer in Fig. 4, it is seen that the mth subcarrier harmonic $X_i^{(m)}$ is weighted by $4/(m\pi)$ and then added to the other inphase harmonics to obtain the input to the inphase symbol accumulator, denoted as X_i. Hence,

$$X_i = \sum_{\substack{m=1 \\ m:odd}}^{L} X_i^{(m)} \frac{4}{m\pi}$$

$$= \sqrt{P_d} d \cos(\phi_c) \frac{8}{\pi^2} \sum_{\substack{m=1 \\ m:odd}}^{L} \frac{\cos(m\phi_{su})}{m^2} + n_{X_i} \quad \text{(A-25)}$$

where

$$n_{X_i} = \frac{4}{\pi} \sum_{\substack{m=1 \\ m:odd}}^{L} \frac{n_A^{(m)} \cos(m\hat{\Theta}_{su}) + n_B^{(m)} \sin(m\hat{\Theta}_{su})}{m} \quad \text{(A-26)}$$

Similarly, the input to the quadrature symbol accumulator, $X_{q,su}$, is obtained by weighing the mth subcarrier harmonic $X_{q,su}^{(m)}$ by $[4/(m\pi)]\sin[(m/2)\pi W_{su}]$ and then adding it to the other quadrature harmonics. Namely,

$$X_{q,su} = \sum_{\substack{m=1 \\ m:odd}}^{L} X_{q,su}^{(m)} \left[\frac{4}{m\pi} \sin\left(\frac{m}{2}\pi W_{su}\right)\right]$$

$$= \sqrt{P_d} d \cos(\phi_c) \frac{8}{\pi^2} \sum_{\substack{m=1 \\ m:odd}}^{L} \sin\left(\frac{m}{2}\pi W_{su}\right) \frac{\sin(m\phi_{su})}{m^2}$$

$$+ n_{X_{q,su}} \quad \text{(A-27)}$$

where

$$n_{X_{q,su}} = \frac{4}{\pi} \sum_{\substack{m=1 \\ m:odd}}^{L} \sin\left(\frac{m}{2}\pi W_{su}\right)$$

$$\times \frac{n_B^{(m)} \cos(m\hat{\Theta}_{su}) - n_A^{(m)} \sin(m\hat{\Theta}_{su})}{m} \quad \text{(A-28)}$$

The variance of n_{X_i} in Eq. (A-26) can be found as

$$\sigma_{n_{X_i}}^2 = \mathbf{E}\left\{\left(\frac{4}{\pi} \sum_{\substack{m=1 \\ m:odd}}^{L} \frac{n_A^{(m)} \cos(m\hat{\Theta}_{su}) + n_B^{(m)} \sin(m\hat{\Theta}_{su})}{m}\right)^2\right\}$$

$$= \left(\frac{4}{\pi}\right)^2 \sum_{\substack{m=1 \\ m:odd}}^{L} \frac{\mathbf{E}\left\{(n_A^{(m)})^2\right\} \cos^2(m\hat{\Theta}_{su}) + \mathbf{E}\left\{(n_B^{(m)})^2\right\} \sin^2(m\hat{\Theta}_{su})}{m^2} \quad \text{(A-29)}$$

where

$$\mathbf{E}\left\{(n_A^{(m)})^2\right\} = \mathbf{E}\left\{(n_B^{(m)})^2\right\} = \frac{N_0}{2} B_{su} \quad \forall m$$

Here, B_{su} is the bandwidth of the filter $H_{su}(z)$ in Fig. 2. The last equality in Eq. (A-29) holds because $n_A^{(m)}$ and $n_B^{(m)}$ are mutually independent with respect to each other as well as their counterparts at other subcarrier harmonics. After letting the highest recorded subcarrier harmonic order L go to infinity, and then using the identity

$$\sum_{\substack{m=1 \\ m:odd}}^{\infty} \frac{1}{m^2} = \frac{\pi^2}{8}$$

it is easily shown that the variance of n_{X_i} approaches twice the variance of either $n_A^{(m)}$ or $n_B^{(m)}$. Therefore, n_{X_i} has a flat, one-sided PSD level equal to N_0 W/Hz, which is twice the PSD level of $n_A^{(m)}$ or $n_B^{(m)}$, within B_{su} Hz. Similarly, it can also be shown that $n_{X_{q,su}}$ in Eq. (A-28) has a flat, one-sided power spectral density level approximately equal to $(W_{su}N_0)$ W/Hz within the lowpass arm filter bandwidth B_{su} Hz. This result is as expected since windowing the quadrature subcarrier reference reduces the noise power by the factor W_{su}.

In referring to Fig. 4, it is seen that the subcarrier loop inphase and quadrature accumulator outputs, Y_i and $Y_{q,su}$, are obtained by averaging samples of X_i and $X_{q,su}$ over a symbol duration. Assuming that ϕ_c and $m\phi_{su}$ for all m are approximately constant over a symbol duration, Y_i and $Y_{q,su}$ are as given by Eqs. (40) and (41). It is also true that, since the one-sided PSD levels of n_{X_i} (N_0 W/Hz) and $n_{X_{q,su}}$ ($[W_{su}N_0]$ W/Hz) are flat over B_{su} Hz and since B_{su} is much greater than the symbol rate ($1/T$), the variance of n_{Y_i} and the variance of $n_{Y_{q,su}}$ are equal to $N_0/(2T)$ and $W_{su}N_0/(2T)$, respectively. Furthermore, since

$$\left\{n_A^{(m)}, n_B^{(m)} \mid \text{ odd integer m }, \ 1 \le m \le L\right\}$$

is a set of mutually independent random samples, it is straightforward to show that n_{X_i} and $n_{X_{q,su}}$ are independent, which in turn assures that n_{Y_i} and $n_{Y_{q,su}}$ are also independent.

IV. Derivation of Eq. (44)

In referring to the suppressed carrier loop in Fig. 4, it is seen that the recorded mth subcarrier harmonic waveforms $SU_{sc}^{(m)}$, $SU_{ss}^{(m)}$, $SU_{cc}^{(m)}$, and $SU_{cs}^{(m)}$ are demodulated as follows:

$$C^{(m)} = SU_{ss}^{(m)}\cos(\hat{\Theta}_c) + SU_{cs}^{(m)}\sin(\hat{\Theta}_c) \qquad \text{(A-30)}$$

$$D^{(m)} = SU_{sc}^{(m)}\cos(\hat{\Theta}_c) + SU_{cc}^{(m)}\sin(\hat{\Theta}_c) \qquad \text{(A-31)}$$

where $\hat{\Theta}_c$ represents the estimated carrier error phase. After substituting Eqs. (17) to (20) into the above equations, it can be found that

$$C^{(m)} = -\sqrt{P_d}\frac{2d}{m\pi}\cos(m\Theta_{su})\cos(\phi_c) + n_C^{(m)} \qquad \text{(A-32)}$$

$$D^{(m)} = -\sqrt{P_d}\frac{2d}{m\pi}\sin(m\Theta_{su})\sin(\phi_c) + n_D^{(m)} \qquad \text{(A-33)}$$

where

$$n_C^{(m)} = n_{SU_{ss}}^{(m)}\cos(\hat{\Theta}_c) + n_{SU_{cs}}^{(m)}\sin(\hat{\Theta}_c) \qquad \text{(A-34)}$$

$$n_D^{(m)} = n_{SU_{sc}}^{(m)}\cos(\hat{\Theta}_c) + n_{SU_{cc}}^{(m)}\sin(\hat{\Theta}_c) \qquad \text{(A-35)}$$

and $n_{SU_{ss}}^{(m)}$, $n_{SU_{sc}}^{(m)}$, $n_{SU_{cs}}^{(m)}$, and $n_{SU_{cc}}^{(m)}$ are as given by Eqs. (21) to (24).

It is clear that both $n_C^{(m)}$ and $n_D^{(m)}$ have a flat, one-sided PSD level equal to $N_0/2$ W/Hz within the frequency interval $[0, B_{su}]$ Hz, since $n_{SU_{ss}}^{(m)}$, $n_{SU_{sc}}^{(m)}$, $n_{SU_{cs}}^{(m)}$, and $n_{SU_{cc}}^{(m)}$ have the PSD level equal to $N_0/2$ W/Hz within the same band. Note that B_{su} is the bandwidth of the filter $H_{su}(z)$ in Fig. 2. It is easy to show that both $n_C^{(m)}$ and $n_D^{(m)}$ are not only independent of each other, but also independent of their counterparts at other subcarrier harmonics. Moreover, it can be shown that

$$\left\{n_A^{(m)}, n_B^{(m)}, n_C^{(m)}, n_D^{(m)} \mid \text{ odd integer m, } 1 \le m \le L\right\} \qquad \text{(A-36)}$$

is a set of mutually independent random samples.

The signals $C^{(m)}$ and $D^{(m)}$ are multiplied by the subcarrier references and then added to remove the subcarrier frequency error. The resulting signal $X_{q,sca}^{(m)}$ is as follows:

$$X_{q,sca}^{(m)} = C^{(m)}\cos(m\hat{\Theta}_{su}) + D^{(m)}\sin(m\hat{\Theta}_{su}) \qquad \text{(A-37)}$$

$$= \sqrt{P_d}\frac{2d}{m\pi}\cos(m\phi_{su})\sin(\phi_c) + n_{X_{q,sca}}^{(m)} \qquad \text{(A-38)}$$

where

$$n_{X_{q,sca}}^{(m)} = n_C^{(m)}\cos(m\hat{\Theta}_{su}) + n_D^{(m)}\sin(m\hat{\Theta}_{su}) \qquad \text{(A-39)}$$

In a manner similar to forming the weighted sums in the subcarrier tracking, the mth subcarrier harmonic, $X_{q,sca}^{(m)}$, is weighted by $4/(m\pi)$ and then added to the other quadrature harmonics to obtain $X_{q,sca}$, the input to the quadrature arm accumulator. Thus,

$$X_{q,sca} = \sqrt{P_d} d \sin(\phi_c) \frac{8}{\pi^2} \sum_{\substack{m=1 \\ m:odd}}^{L} \frac{\cos(m\phi_{su})}{m^2} + n_{X_{q,sca}} \tag{A-40}$$

where

$$n_{X_{q,sca}} = \frac{4}{\pi} \sum_{\substack{m=1 \\ m:odd}}^{L} \frac{n_C^{(m)} \cos(m\hat{\Theta}_{su}) + n_D^{(m)} \sin(m\hat{\Theta}_{su})}{m} \tag{A-41}$$

Using the same procedure as in the derivation of the PSD level of n_{X_i}, it can be easily verified that $n_{X_{q,sca}}$ has a PSD level approximately equal to N_0 W/Hz within the frequency interval $[0, B_{su}]$ Hz. In referring to Fig. 4, it is seen that the suppressed carrier loop quadrature arm accumulator output, $Y_{q,sca}$, is obtained by averaging samples of $X_{q,sca}$ over a symbol duration. Assuming that ϕ_c and $m\phi_{su}$, for all m, are approximately constant over a symbol duration, the signal $Y_{q,sca}$ is as given in Eq. (44). Furthermore, assuming that B_{su} is much greater than the symbol rate $(1/T)$, the variance of $n_{Y_{q,sca}}$ can be shown to be equal to $N_0/(2T)$.

By using Eq. (A-36), it is straightforward to show that n_{X_i} and $n_{X_{q,sca}}$ are independent, which in turn assures that n_{Y_i} and $n_{Y_{q,sca}}$ are independent.

Table 1. Loss in data power as a function of subcarrier harmonics.

Highest recorded subcarrier harmonic, L	Number of subcarrier harmonics at A/D output, n	Loss, dB
1	1	0.91
3	2	0.45
5	3	0.30
7	4	0.22
9	5	0.18

Table 2(a). Required number of operations for the demodulation function (n is the number of harmonics recorded).

Mode	Multiplication operations per sample	Multiplication operations per symbol	Addition operations per sample	Addition operations per symbol	Lookup table
Residual carrier with subcarrier	$6 + 8n$	14	$13 + 6n$	24	$4 + 2n$
Suppressed carrier with subcarrier	$4 + 14n$	14	$12 + 10n$	25	$4 + 2n$
Suppressed carrier with no subcarrier	6	12	10	17	4

Table 2(b). Detailed list of operations.

Three modes with types of operations for each	Number of multiplication operations per sample	Number of multiplication operations per symbol	Number of addition operations per sample	Number of addition operations per symbol	Lookup table
Residual carrier with subcarrier					
Residual carrier phase detector	2	0	1	0	0
Residual carrier accumulator	0	0	1	0	0
Residual carrier loop filter	0	3	0	5	0
Residual carrier numerically controlled oscillator	0	1	1	1	2
Subcarrier phase detector	$8n$	0	$2 + 6n$	0	0
Subcarrier accumulator	0	0	0	1	0
Subcarrier loop filter	0	3	0	5	0
Subcarrier numerically controlled oscillator	0	1	1	1	$2n$
Symbol synchronization phase detector	0	1	1	1	0
Symbol synchronization accumulator	0	0	0	1	0
Symbol synchronization loop filter	0	3	0	5	0
Symbol synchronization numerically controlled oscillator	0	1	1	1	2
Residual carrier lock detector	2	0	2	0	0
Subcarrier lock detector	2	0	2	0	0
Split-symbol SSNR estimator	0	1	1	3	0
Total	$6 + 8n$	14	$13 + 6n$	24	$4 + 2n$
Suppressed carrier with subcarrier					
Carrier/subcarrier phase detector	$14n$	0	$3 + 10n$	0	0
Carrier/subcarrier accumulator	0	0	0	2	0
Carrier/subcarrier loop filter	0	6	0	10	0
Carrier/subcarrier numerically controlled oscillator	0	2	2	2	$2 + 2n$
Symbol synchronization phase detector	0	1	1	1	0
Symbol synchronization accumulator	0	0	0	1	0
Symbol synchronization loop filter	0	3	0	5	0
Symbol synchronization numerically controlled oscillator	0	1	1	1	2
Suppressed carrier lock detector	2	0	2	0	0
Subcarrier lock detector	2	0	2	0	0
Split-symbol SSNR estimator	0	1	1	3	0
Total	$4 + 14n$	14	$12 + 10n$	25	$4 + 2n$
Suppressed carrier with no subcarrier					
Suppressed carrier phase detector	4	1	4	0	0
Suppressed carrier accumulator	0	1	0	0	0
Suppressed carrier loop filter	0	3	0	5	0
Suppressed carrier numerically controlled oscillator	0	1	1	1	2
Symbol synchronization phase detector	0	1	1	1	0
Symbol synchronization accumulator	0	0	0	1	0
Symbol synchronization loop filter	0	3	0	5	0
Symbol synchronization numerically controlled oscillator	0	1	1	1	2
Suppressed carrier lock detector	2	0	2	0	0
Split-symbol SSNR estimator	0	1	1	3	0
Total	6	12	10	17	4

Table 3. Throughput comparison (*n* is the number of harmonics recorded).

System	SPECfp92	Percent throughput utilized ($n = 3$)	Percent throughput utilized ($n = 5$)
Sun SS-2	22.8	100	151
Sun SS-10/30	52.9	43	65
Sun SS-10/41	64.7	35	53
Sun SS-10/52	71.4/CPU	32 (on one CPU)	48 (on one CPU)
SGI Crimson	63.4	36	54
HP 710	47.6	48	72
HP 750	75.0	30	45
IBM 340	51.9	44	66
IBM 560	85.6	27	41
Intel Xpress (486)	14.0	160	242

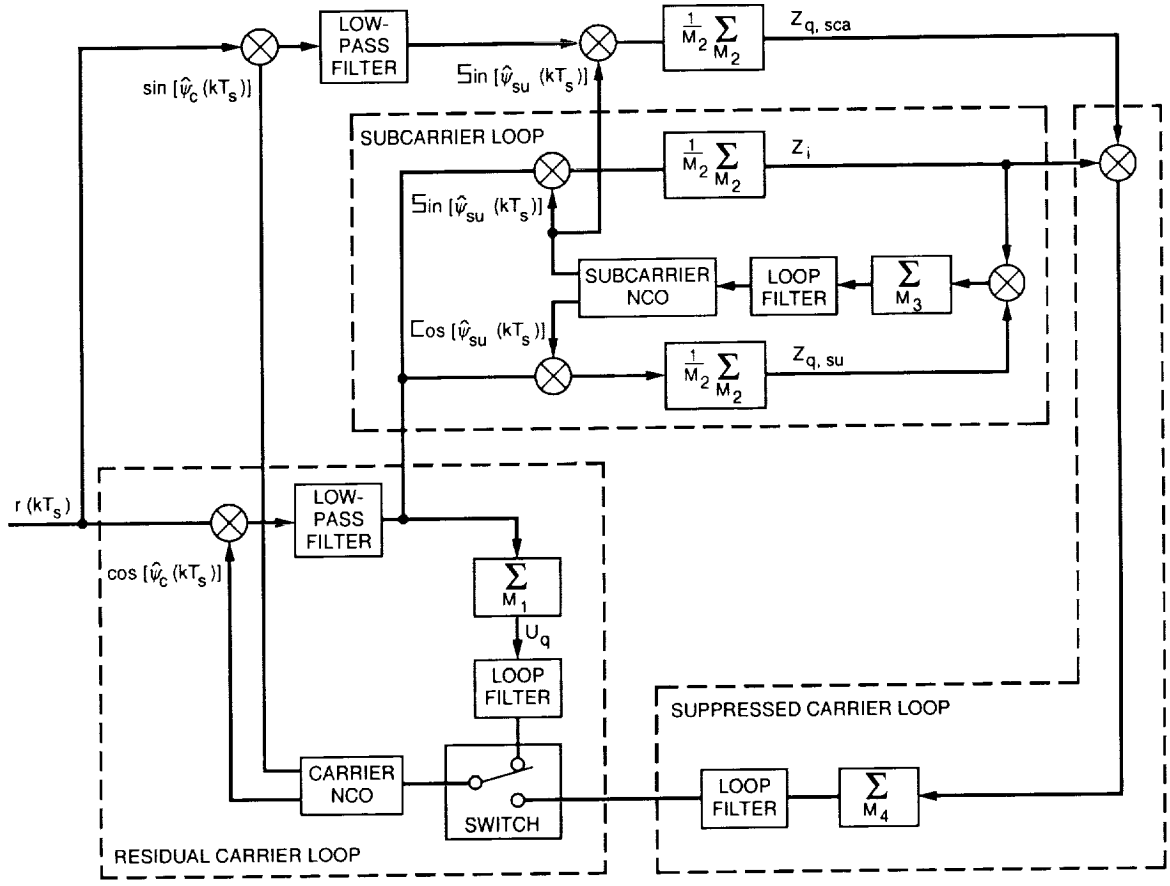

Fig. 1. A simplified block diagram of the ARX II.

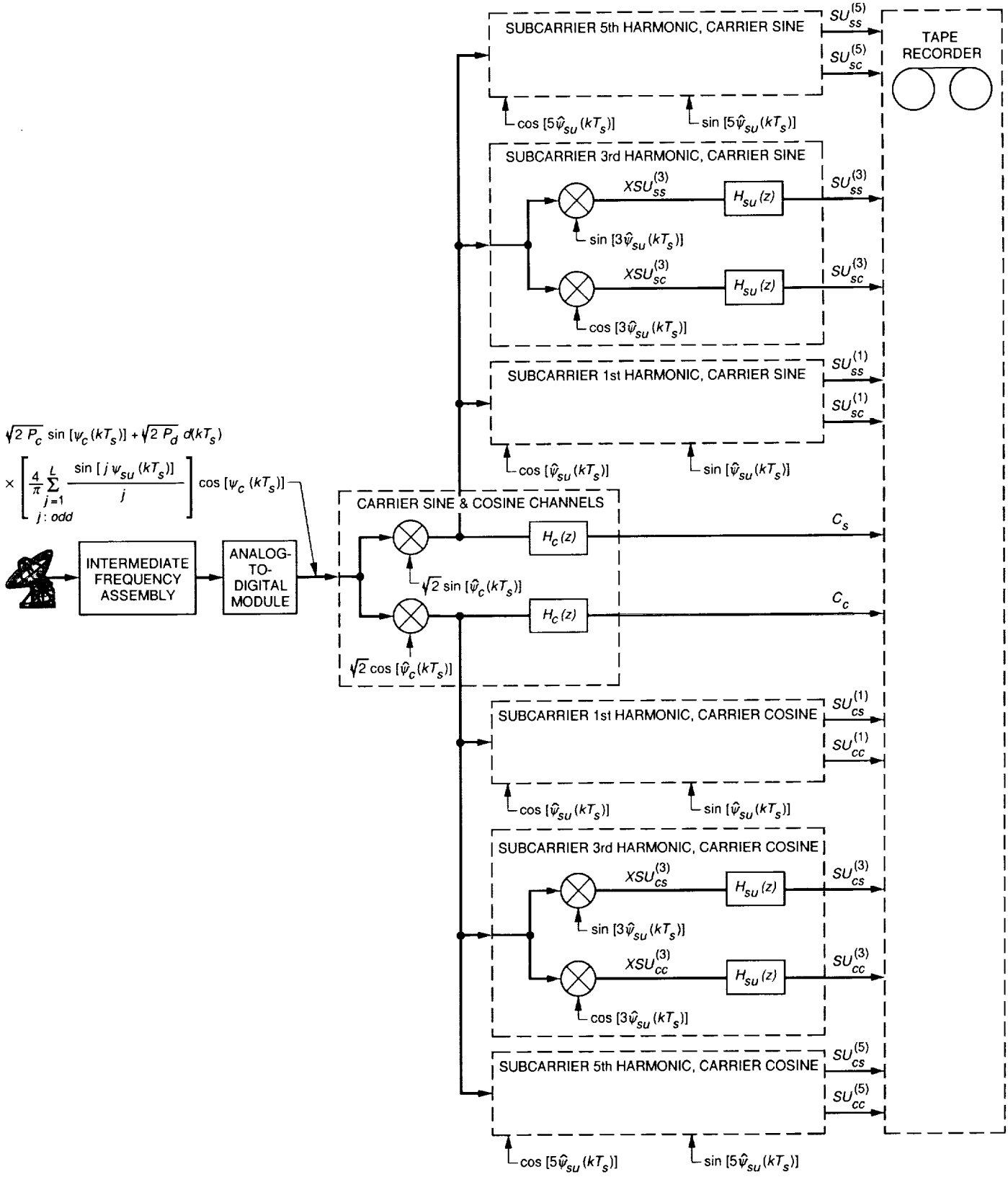

Fig. 2. The two-stage downconversion recording scheme.

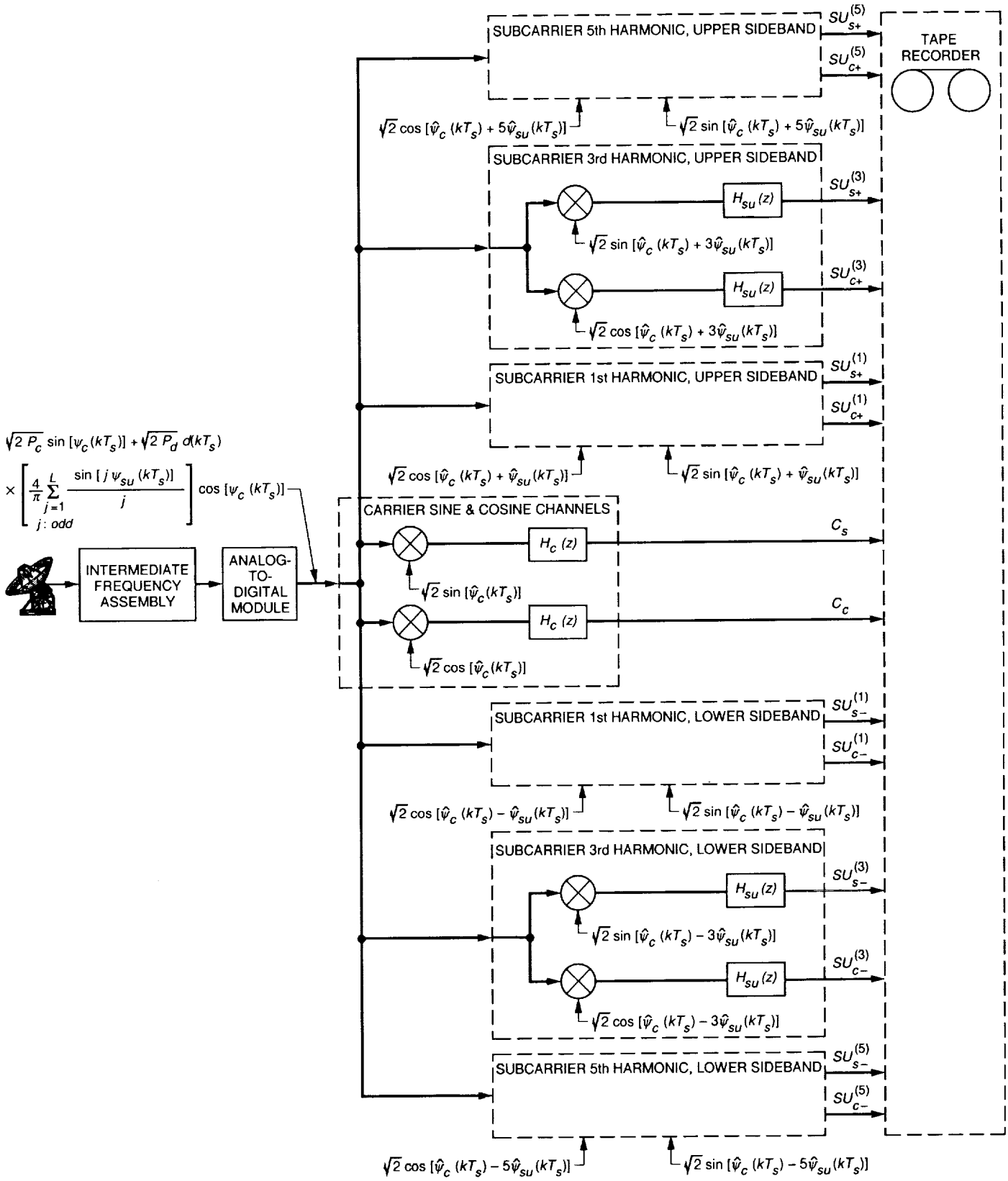

Fig. 3. The direct downconversion recording scheme.

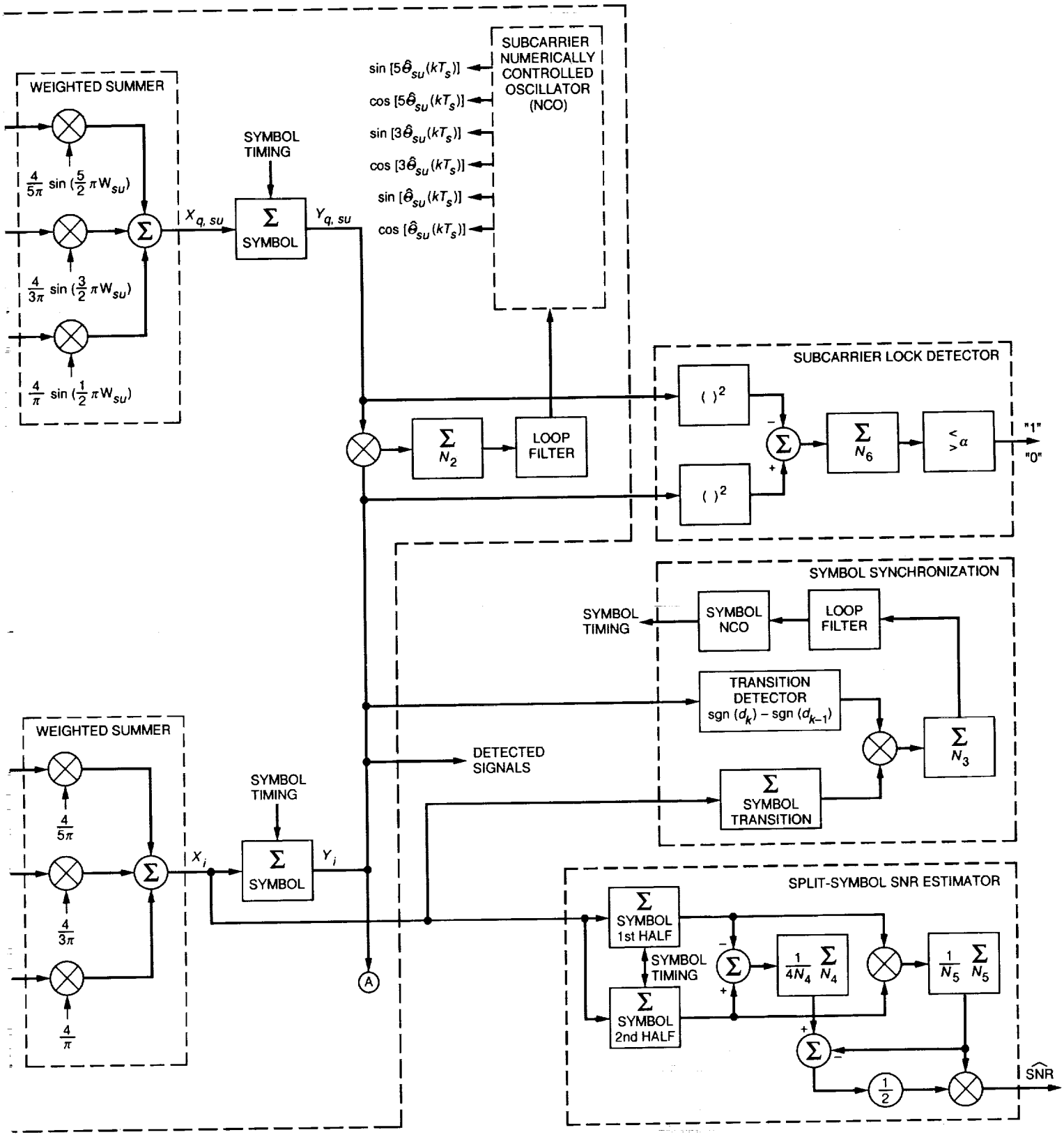

Fig. 4. The coherent baseband demodulator for the two-stage recording scheme.

FOLDOUT FRAME 2

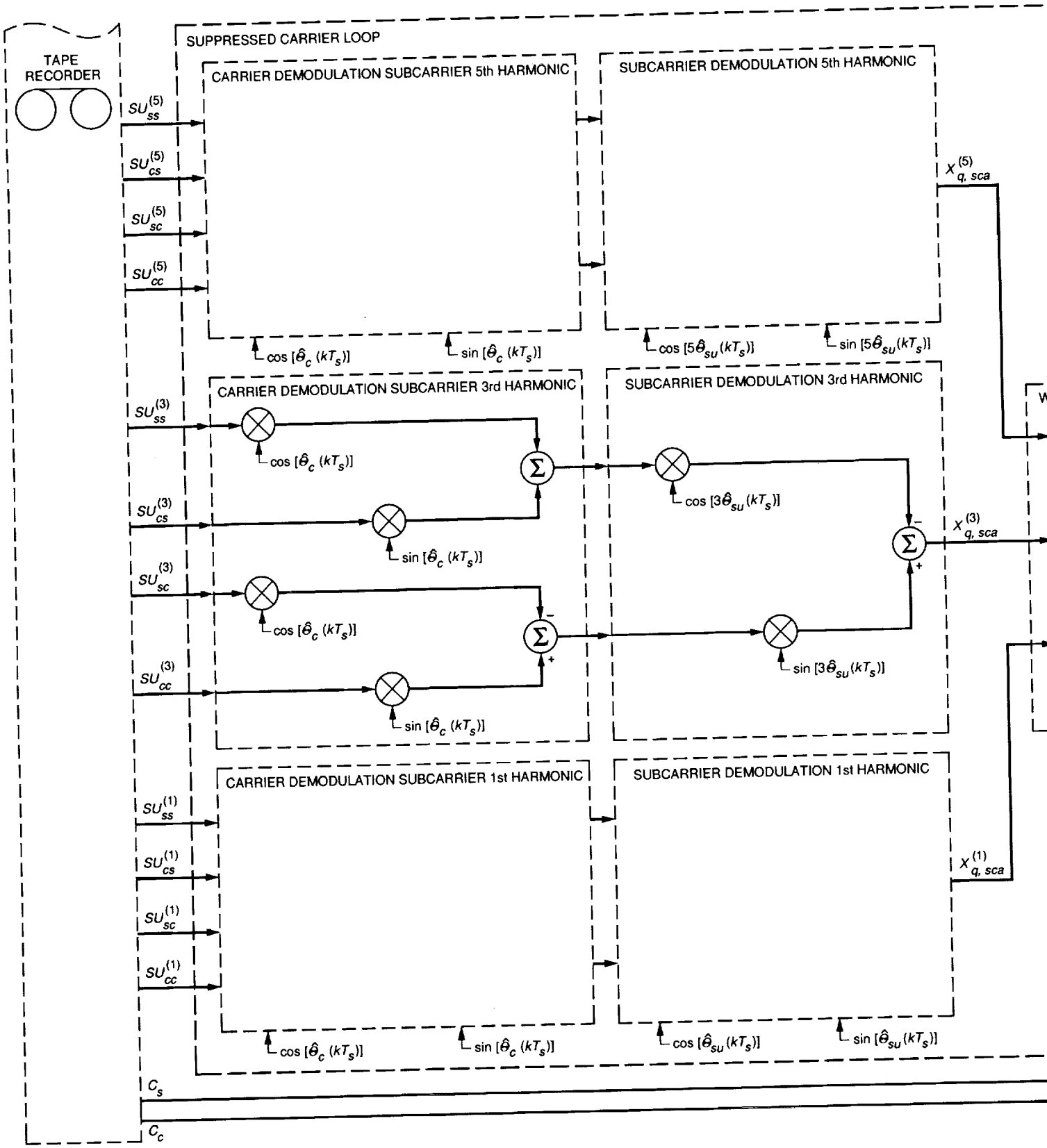

Fig. 4 (contd).

FOLDOUT FRAME

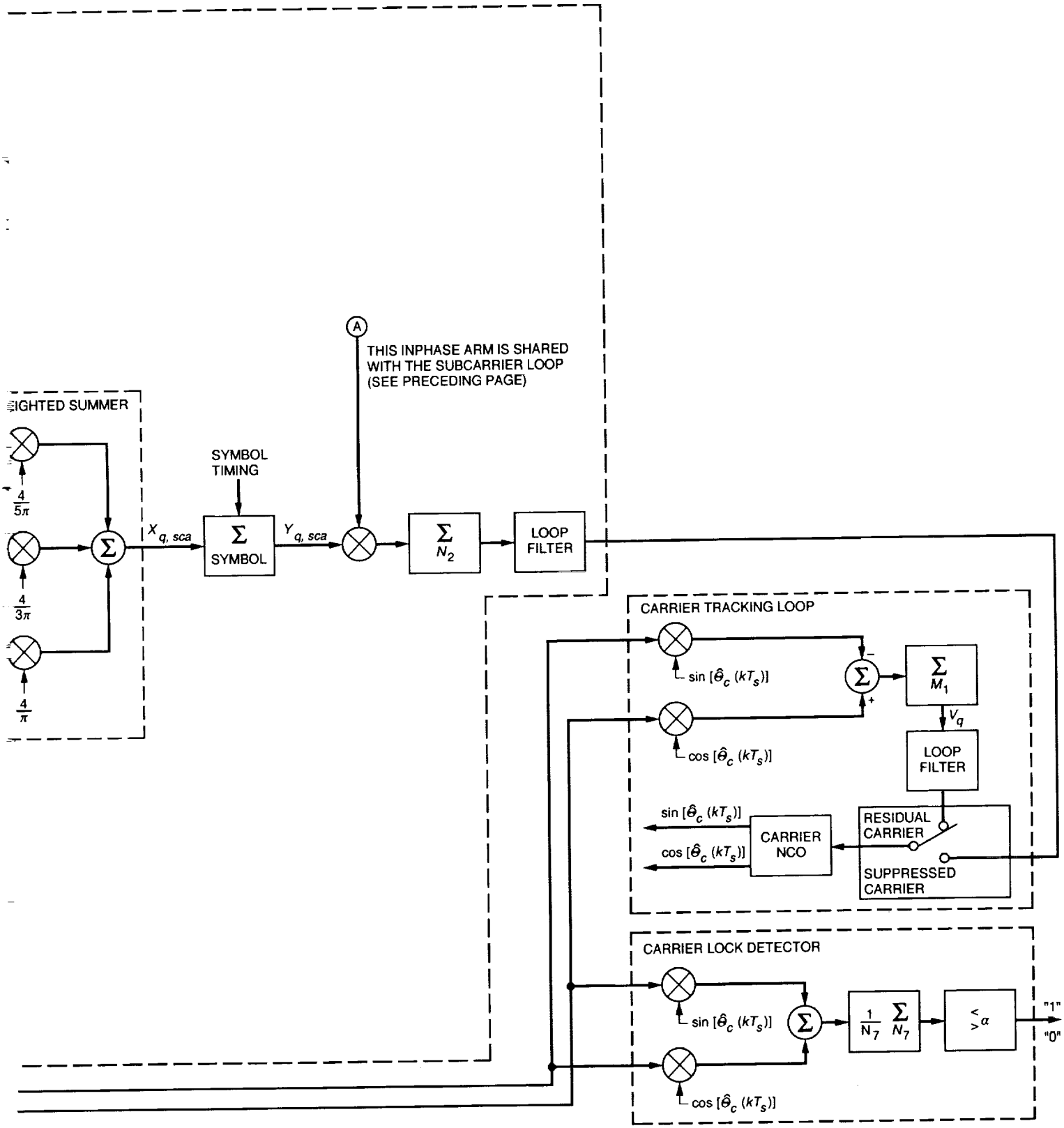

FOLDOUT FRAME 2

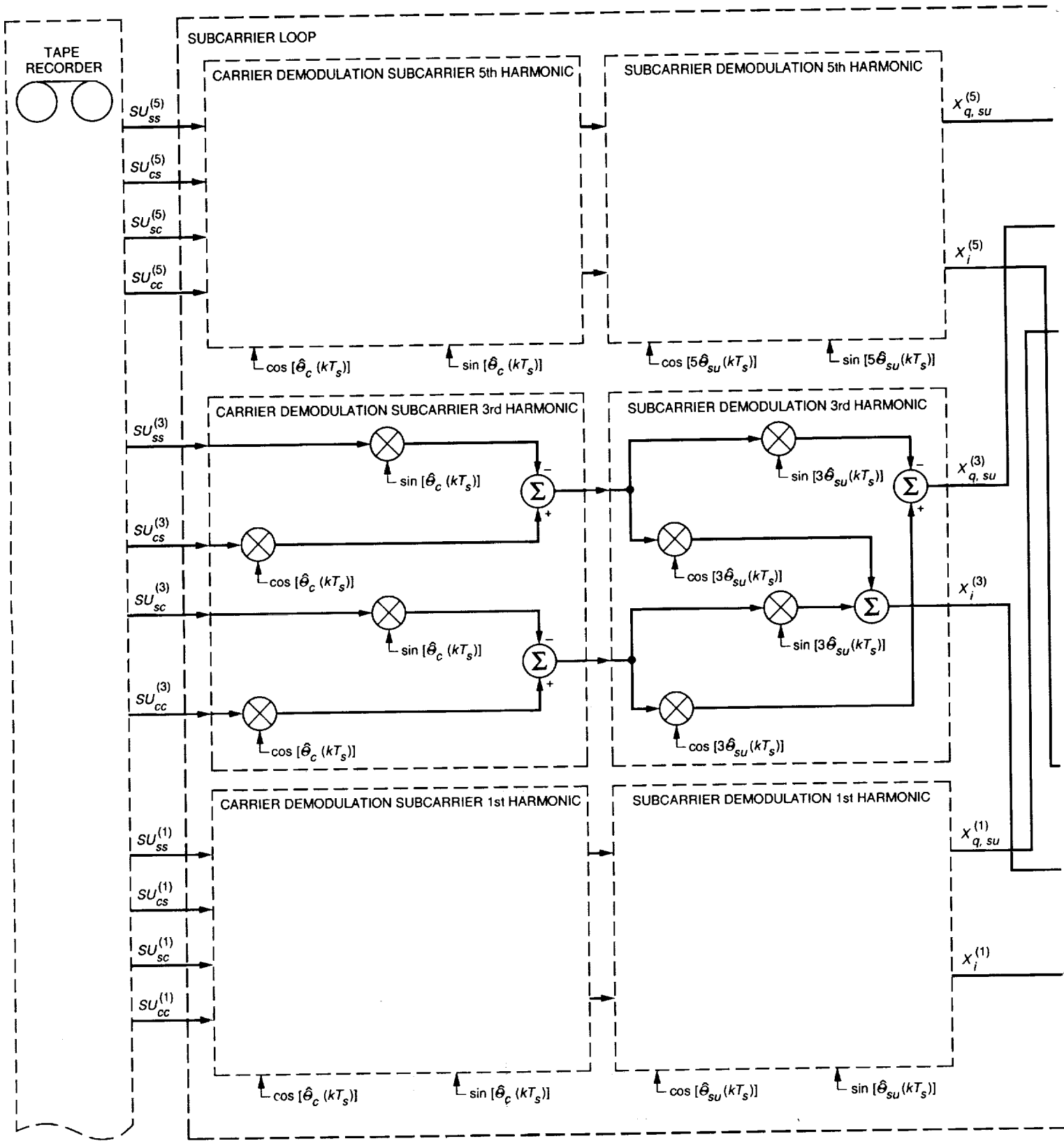

FOLDOUT FRAME

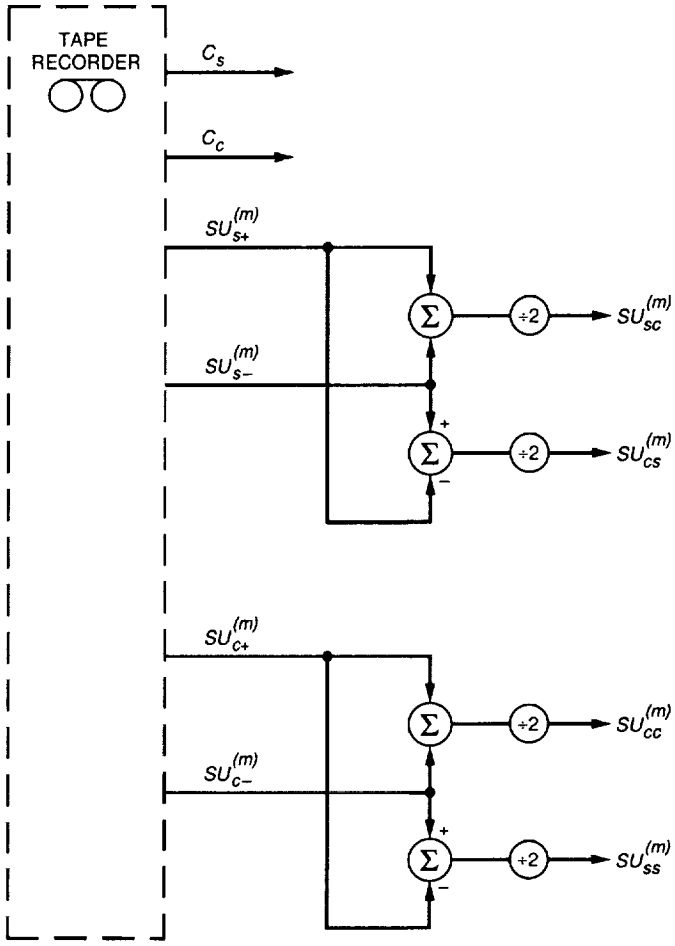

Fig. 5. The processing required to generate the signals $SU_{ss}^{(m)}$, $SU_{sc}^{(m)}$, $SU_{cs}^{(m)}$, $SU_{cc}^{(m)}$ from the signals $SU_{s+}^{(m)}$, $SU_{s-}^{(m)}$, $SU_{c+}^{(m)}$, and $SU_{c-}^{(m)}$.